Articles
doi.org/10.1002/batt.202100025

Chemistry Europe
European Chemical Societies Publishing

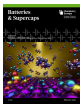

The (In-)Stability of the Ionic Liquids [(TMEDA)BH_2][TFSI] and –[FSI] on the Li(001) Surface

Jonathan Clarke-Hannaford,[a, b] Michael Breedon,*[b] Thomas Rüther,[c] Patrik Johansson,[d] and Michelle J. S. Spencer*[a]

Electrolytes that can enable the use of a Li metal anode at a vast 3860 mAh/g, in place of currently used graphite anodes (372 mAh/g), are required for the advancement of next-generation rechargeable Li batteries. Both quaternary ammonium and boronium (trimethylamine)(dimethylethylamine)dihydroborate $[NNBH_2]^+$ cation-based ionic liquids (ILs) show high electrochemical stability windows and thermal stability for use in Li batteries. Cyclization of the former cation shows improved electrolyte stability compared to the open-chain counterpart. However, it is not known whether this is the case for the cyclic derivative of $[NNBH_2]^+$, *N*,*N*,*N*′,*N*′-tetramethylethylenediamine)dihydroborate $[(TMEDA)BH_2]^+$. Here, the details of the initial stages of solid–electrolyte interphase (SEI) layer formation on a lithium metal surface, Li(001), for the $[(TMEDA)BH_2]^+$ based ILs are revealed using density functional theory (DFT) calculations and *ab initio* molecular dynamics (AIMD) simulations. These indicate that $[(TMEDA)BH_2]^+$ remains intact, displaying a similarly weak interaction with the Li metal surface as the open-chain analogue. The chemical stability shown by the boronium cation indicates spontaneous and unwanted side reactions with the Li anode are unlikely to occur, which could help to facilitate long-term cycling stability of the battery. Altogether, the findings suggest the $[(TMEDA)BH_2]^+$ ILs, like their $[NNBH_2]^+$ IL counterparts, are viable candidates for rechargeable Li metal batteries.

1. Introduction

There are significant efforts being made to develop next-generation rechargeable battery technologies that use a lithium metal anode, referred to as lithium metal batteries (LMBs), rather than the graphite used in today's omnipresent lithium-ion batteries (LIBs). This is mainly due to the 10-fold increase in theoretical gravimetric capacity (3860 *vs.* 372 mAh/g) offered by lithium. At the same time, a successful implementation would also pave the way for other battery technologies that rely on a lithium metal anode, *e.g.* lithium–oxygen/air (Li–O_2) and lithium–sulfur (Li–S) batteries. The high energy densities ultimately made possible would enable a much wider range of applications to be electrified and enhance those that already are. However, there is a crucial obstacle in that a suitable electrolyte is missing, as conventional organic solvent-based electrolytes decompose at the Li metal surface.[1] IL based electrolytes have in general been proposed to offer several advantages, such as inherent safety (negligible vapor pressure), which also enables wider operating temperature windows that in turn reduces parasitic energy losses associated with thermal control. Additionally, IL-based electrolytes may enhance the lithium stripping/plating efficiency and mitigate dendrite growth by forming a flexible and robust passivating thin film known as a solid electrolyte interphase (SEI) layer,[2] also allowing for high current densities and commercially viable lifetimes for LMBs.[2a,3]

The IL cation and anion can be optimized independently to improve both the chemical and physical properties of the electrolytes.[4] Although numerous studies have considered the physicochemical properties obtained with specific ions, few definitive studies are available. To progress further, especially with respect to IL-based electrolytes that can stabilize the Li metal anode and extend the lifetime of LMBs, development of suitable IL cations that influence the formation of a beneficial SEI layer are vital. Previous studies investigating possible thermal[5] and electrochemical[6] induced decomposition of IL cations on the Li anode have focused primarily on pyrrolidinium-based systems. It is not known how other IL cations can influence the formation of a beneficial SEI layer. Few cation families are, however, suitable for sustained cycling of LMBs and these include: quaternary ammonium (NR_4),[7] pyrrolidinium (Pyr),[4,8] piperidinium (Pip),[9] phosphonium (PR_4),[10] and the far less prominent boronium cations.[3a,11] Pyr- and PR_4-based IL electrolytes have achieved stable cycling in Li|Li and Li|

[a] *J. Clarke-Hannaford, Prof. M. J. S. Spencer*
School of Science
RMIT University
GPO Box 2476, Melbourne, Victoria 3001, Australia
E-mail: michelle.spencer@rmit.edu.au
[b] *J. Clarke-Hannaford, Dr. M. Breedon*
Manufacturing
CSIRO
Research Way, Clayton, Victoria 3168, Australia
E-mail: michael.breedon@csiro.au
[c] *Dr. T. Rüther*
Energy
CSIRO
Research Way, Clayton, Victoria 3168, Australia
[d] *Prof. P. Johansson*
Department of Physics
Chalmers University of Technology
SE-412 96, Göteborg, Sweden

Supporting information for this article is available on the WWW under https://doi.org/10.1002/batt.202100025

$LiFePO_4$ cells[2a,8a,12] through the formation of a stable and uniform SEI layer. The composition and structure of such layered thin films is highly dynamic; being dependent upon the electrolyte components, and the duration that the anode is in contact with the electrolyte.[2a,13] Formation of the SEI on the lithium anode will generally consist of two layers.[10a,13c,d,14] The first is the compact (~nm thick) inorganic inner layer dominated by species such as LiF and Li_2O[10a,15] that originate from the decomposition of electrolyte components such as the IL itself and Li-salt anions (e.g. bis(trifluoromethanesulfonyl) imide $[TFSI]^-$ or bis(fluorosulfonyl)imide $[FSI]^-$).[16] The second is the larger outer layer that builds upon the inner layer, consisting of inorganic and organic IL decomposition species, along with embedded anions and cations.[10a,17] For the trimethyl(isobutyl)phosphonium ($[P_{111i4}]$) [FSI] IL, experimental characterization of the SEI layer indicated only decomposition products attributed to the anion were present.[10a] It was found the phosphonium cation would become embedded, most likely remaining intact, in the outer organic layer.[10a] In contrast, previous studies have determined decomposition products of *N*-methyl-*N*-butylpyrrolidinium ($[Pyr_{14}]^+$) and *N*-methyl-*N*-propylpyrrolidinium ($[Pyr_{13}]^+$) cations to be a part of the SEI layer composition. For the $[Pyr_{13}]$[FSI]/Li[FSI] electrolyte, possible abstraction of hydrogen from the cation was indicated by the presence of LiOH in the inner-SEI layer,[2a,15b] while methyl- and propyl pyrrolidine were also shown to occur in the outer organic layer.[2a] For $[Pyr_{14}]$[TFSI], a recent study deduced *N*-butyl-*N*-methyl-*N*-but-3-eneamine is one of the decomposition products of the cation formed in the outer organic layer.[18] This particular product has the potential to enable polymerized species to form which have been reported to imbue desirable elastomeric properties to the SEI layer.[18] Computational modelling of the $[Pyr_{13}]$[FSI][15b] and $[Pyr_{14}]$[TFSI][15a,c] ILs on the Li(001) surface further supported the domination of chemical species attributed to the anion forming the inner inorganic component of the SEI layer. Additionally, these studies predicted the pyrrolidinium cations to remain intact during the early stages of SEI layer formation.[15]

The boronium-based $[NNBH_2]$[TFSI] IL-based electrolyte has shown better cycling performance than even the well-known $[Pyr_{14}]$[TFSI] IL-based electrolytes.[3a] Computational modelling of the pure $[NNBH_2]$[TFSI] IL on the Li surface found the $[NNBH_2]^+$ cation does not decompose on the Li(001) anode surface during the initial stages of the SEI formation,[19] similar to $[Pyr_{13}]^+$ and $[Pyr_{14}]^+$. It has been suggested that replacing a hydrogen atom on the boron center with an alkyl group or cyclization to a 5-membered ring could alter the chemical stability and electrochemical behavior.[11] Here we investigate this by using ILs based on the 'cyclic' boronium cation N,N,N′,N′-tetramethylethylenediamine)dihydroborate (also referred to as 1,1,3,3-tetramethyl-1,3λ,[4] 2-diazaborolidin-1-ium[20]) ($[(TMEDA)BH_2]^+$) and $[TFSI]^-$ and $[FSI]^-$ as counter ions to further understand possible decomposition and reaction mechanisms occurring at the IL/Li(001) surface using DFT calculations and AIMD simulations at elevated temperatures.

Methodology

Electronic and structural properties for the IL/Li(001) systems were calculated using DFT as implemented in the Vienna *ab initio* Simulation Package (VASP) 5.4.4,[21] applying the projector–augmented wave (PAW) method[22] and the generalized gradient approximation (GGA) of Perdew, Burke and Ernzerhof.[23] To account for van der Waals forces, the DFT-D3 functional of Grimme *et al.*[24] was used. All systems were relaxed so that the Hellmann-Feynman force was $\leq 0.01\ eV \cdot Å^{-1}$ and the total energy $\leq 10^{-4}$ eV. A 7 layer Li(001)-[4×4] surface was used to represent the anode surface; for details see previous studies.[1b,15b,19,25] For all systems using the Li(001) surface, a 4×4×1 Gamma centered *k*-point mesh was used with a cut–off energy of 550 eV.

A total of 14 and 13 initial adsorption sites and orientations of $[(TMEDA)BH_2]$[TFSI] and –[FSI] ion-pairs, respectively, were investigated on the Li surface to sample possible configurations. These initial structures were selected so that atop, bridge and hollow adsorption sites for the anion and cation were evaluated. The IL ion-pairs were initially placed > 2.5 Å from the uppermost layer of Li surface atoms. Density of state (DOS) calculations were performed for the optimized structures. Binding energies, E_b, for the ILs adsorbed on the Li(001) surface were calculated as [Eq. (1)]:

$$E_b = E_{tot}(IL \dot{s} Li) - [E_{tot}(IL) + E_{tot}(Li)] \quad (1)$$

where $E_{tot}(IL \cdot Li)$ is the total energy of a system containing the Li(001) surface and the IL; $E_{tot}(Li)$ is the total energy of the optimized clean Li(001) surface; E_{tot} (IL) is the total energy of the optimized isolated IL ion-pair. The partial charges for the individual atoms were calculated according to the Bader charge analysis method.[26] The electron localization function (ELF) plots[27] were included to provide a representation of the electron localization to better interpret the bond type and order for the IL/Li(001) systems, as the ELF gives an indication of the likelihood of formation of bonding and nonbonding electron pairs.

Constrained geometry optimization calculations were performed to estimate the barrier for dissociation of the $[(TMEDA)BH_2]^+$ cation on the Li(001) surface. This approach involved removing a hydrogen atom attached to the $–BH_2$ and $–CH_3$ groups of the cation.

The AIMD simulations were performed using VASP[21] with the NVT ensemble, with three different simulation temperatures (298, 358 and 428 K) controlled by the Nosé thermostat.[28] A time step of 0.5 fs was implemented in the simulations. A Verlet algorithm was used to integrate the equations of motion. The most stable IL/Li(001) structures were used as the initial starting configurations with the atoms in the bottom two layers of the Li(001) surface being kept fixed during all AIMD simulations and DFT calculations.

2. Results and Discussion

In the first part of this work, adsorption of the ILs on the Li surface was modelled using DFT to determine the possible reactions and associated electronic properties. The findings are compared to those obtained for the open-chain boronium cation.[19] In the second part of the work, AIMD simulations were used to determine the effect of temperature on the IL/Li reactions and the decomposition products as a function of temperature. Finally, the possibility of decomposition of the cation was examined.

2.1. DFT Calculations of the IL/Li(001) Interface

2.1.1. [(TMEDA)BH_2][TFSI]/Li(001)

Eleven unique stable structures were obtained for [(TMEDA)BH_2][TFSI]/Li(001) and, based on their binding energies and adsorption geometries, were classified into four discrete orientations (named **I_{BT}**, **II_{BT}**, **III_{BT}** and **IV_{BT}**). The most stable structure for each orientation is shown in Figure 1, with the associated binding energy values presented in Table S1. The other structures are depicted in Figure S1.

Five structures were found to adsorb in Orientation **I_{BT}** (**I_{BT}A-E**) with the anion and cation adsorbing next to each other on the surface with binding energies ranging between −2.35 to −1.78 eV (Table S1). In this orientation, the anion forms two bonds to surface Li, via each of the oxygen atoms in the $-SO_2$ group. The Li–O bonds formed are 1.89 and 1.92 Å, which is within 0.08 and 0.11 Å of the Li–O bonds in solid Li_2O (2.00 Å) PDF 00-004-0857 (ICCD, 2018).[29] The accumulation of charge on the oxygen atoms and depletion on the Li atoms seen in the ELF plots (Figure 1) indicate the formation of ionic bonds, which is consistent with the bond lengths and strong binding energy values. The ELF in the region between the cation and Li surface, while not perturbed greatly, does change, which is consistent with a weak interaction between the cation and the surface. In this orientation, charge is withdrawn from the surface by both the anion and cation, also consistent with both species of the IL interacting with the surface.

For Orientation **II_{BT}** (structures **II_{BT}A-B**), the IL adsorbs so that the anion forms one (ionic) bond to the surface, between one of the oxygen atoms on the $-SO_2$ group and a surface Li atom. The cation also interacts weakly with the surface via the hydrogen atoms at the boron center. Again, there is a transfer of charge from the Li surface to both the cation and anion. This Orientation is weaker than Orientation **I_{BT}** as the anion only forms one bond to the surface.

For Orientation **III_{BT}** (structure **III_{BT}A**), the anion forms two bonds to the surface. As opposed to Orientation **I_{BT}** (where the Li–O bonds formed were from oxygen atoms on a single $-SO_2$ group), this orientation has the two bonds formed from an oxygen atom on both $-SO_2$ groups. The binding is weaker for this orientation as the cation adsorbs above the anion and does not interact directly with the surface. In this orientation, there is an overall withdrawal of charge from the surface, but it is smaller than for Orientations **I_{BT}** or **II_{BT}**, consistent with the weaker binding. Further, the charge on the cation does not change after adsorption, indicating it is only the anion that interacts with the surface.

For Orientation **IV_{BT}** (structures **IV_{BT}A-C**), the cation adsorbs on the surface with the anion located above the cation. It is the hydrogen atoms on the $-BH_2$ group and the neighboring $-CH_3$ groups that interact with the Li surface. While there is an overall net withdrawal of charge from the surface, the charge on the anion does not change, consistent with its location above the anion where it does not interact with the Li substrate.

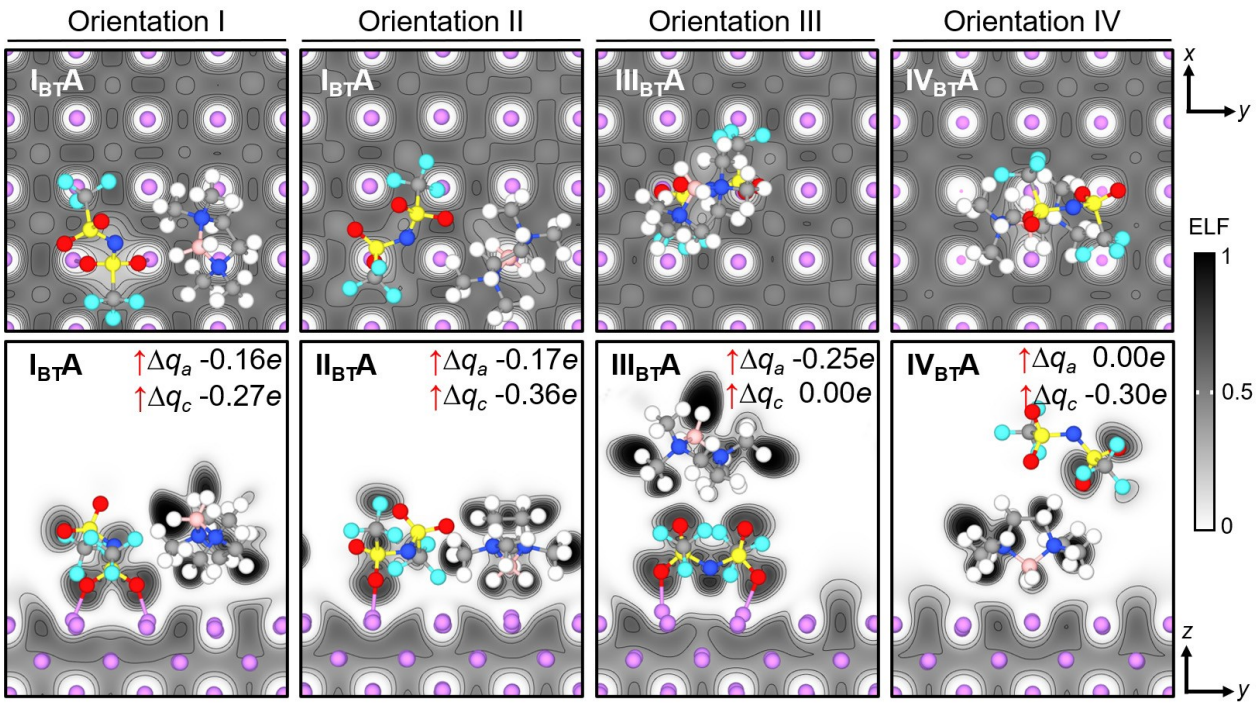

Figure 1. The most stable structures (**I_{BT}A**, **II_{BT}A**, **III_{BT}A** and **IV_{BT}A**) of the four different orientations of [(TMEDA)BH_2][TFSI]/Li(001) are shown with an ELF slice cut through the top most Li surface layers. High regions of ELF (values near 1) can be interpreted as bonding and nonbonding electron pairs. Δq_a and Δq_c represent the charge transferred to the anion and cation, respectively. (Li, F, N, O, S, C, H, B atoms shown in purple, cyan, blue, red, yellow, grey, white and pink, respectively).

When compared to the open-chain boronium-based IL,[19] the cyclic cation absorbs in similar orientations, favoring the formation of Li–O bonds.

Orientations $\mathbf{I}_{BT}$ and $\mathbf{II}_{BT}$ are shown to have stronger binding energies when compared to $\mathbf{III}_{BT}$ and $\mathbf{IV}_{BT}$, due to the strong interaction of both the anion and the cation with the Li surface. The adsorption sites and orientation of the ion-pair in the $\mathbf{I}_{BT}$ and $\mathbf{II}_{BT}$ structures also leads to an increased withdrawal of charge from the Li surface, between −0.56 to −0.35*e*, when compared to Orientations $\mathbf{III}_{BT}$ (−0.25*e*) and $\mathbf{IV}_{BT}$ (−0.30*e*).

The density of states (DOS) is shown for the individual ion-pairs and clean Li(001) surface in Figure S2, while the DOS for the most stable structures of each orientation ($\mathbf{I}_{BT}\mathbf{A}$, $\mathbf{II}_{BT}\mathbf{A}$, $\mathbf{III}_{BT}\mathbf{A}$ and $\mathbf{IV}_{BT}\mathbf{A}$) are shown in Figure S3.

After adsorption of the ion-pair on the surface, the ion-pair states for all structures are shifted in energy, consistent with a relaxation of states upon adsorption. There is also a strong overlap of states with the surface between ~1 to 4.5 eV which explains the interaction between both ions with the surface. The intensity of the anion states is greatest for structures $\mathbf{I}_{BT}\mathbf{A}$, $\mathbf{II}_{BT}\mathbf{A}$ and $\mathbf{III}_{BT}\mathbf{A}$ where the anion is interacting more strongly with the surface. When the cation adsorbs closer to the surface (such as for $\mathbf{IV}_{BT}\mathbf{A}$) the states attributed to the cation are stronger. Further, the changes in intensity and energy of the anion-based states are smaller, consistent with the weaker interaction with the surface for this adsorption orientation.

Overall, [(TMEDA)BH_2][TFSI] binds more strongly to the Li(001) surface (−2.35 eV) than does [NNBH_2][TFSI] (−1.95 eV),[19] however, the difference is relatively small.

2.1.2. [(TMEDA)BH_2][FSI]/Li(001)

For [(TMEDA)BH_2][FSI]/Li(001), eleven unique structures were obtained and can again be classified into four discrete orientations ($\mathbf{I}_{BF}$-$\mathbf{IV}_{BF}$). The most stable of these are shown in Figure 2. The others are presented in Figure S4, along with their electronic properties in Table S2.

For Orientation $\mathbf{I}_{BF}$ (structures $\mathbf{I}_{BF}\mathbf{A}$-$\mathbf{B}$), the $[FSI]^-$ anion was found to decompose on the surface during the geometry optimization. Two decomposition pathways were found, each involving two steps, which resulted in different products having similar binding energy values.

The first reaction pathway (for $\mathbf{I}_{BF}\mathbf{A}$) involved breaking of one of the S–F bonds on the $-SO_2F$ groups, followed by breaking the S–F on the remaining $-SO_2F$ group according to the following reaction [Eq. (2)]:

$$[(TMEDA)BH_2]^+ + [FSI]^- \rightarrow (TMEDA)BH_{2(ads)} + SO_2NSO_2F_{(ads)}$$
$$+F_{(ads)} \rightarrow (TMEDA)BH_{2(ads)} + N(SO_2)_{2(ads)} + 2F_{(ads)} \quad (2)$$

The two fluorine atoms then formed bonds with three Li surface atoms each while the remaining $N(SO_2)_2$ fragment

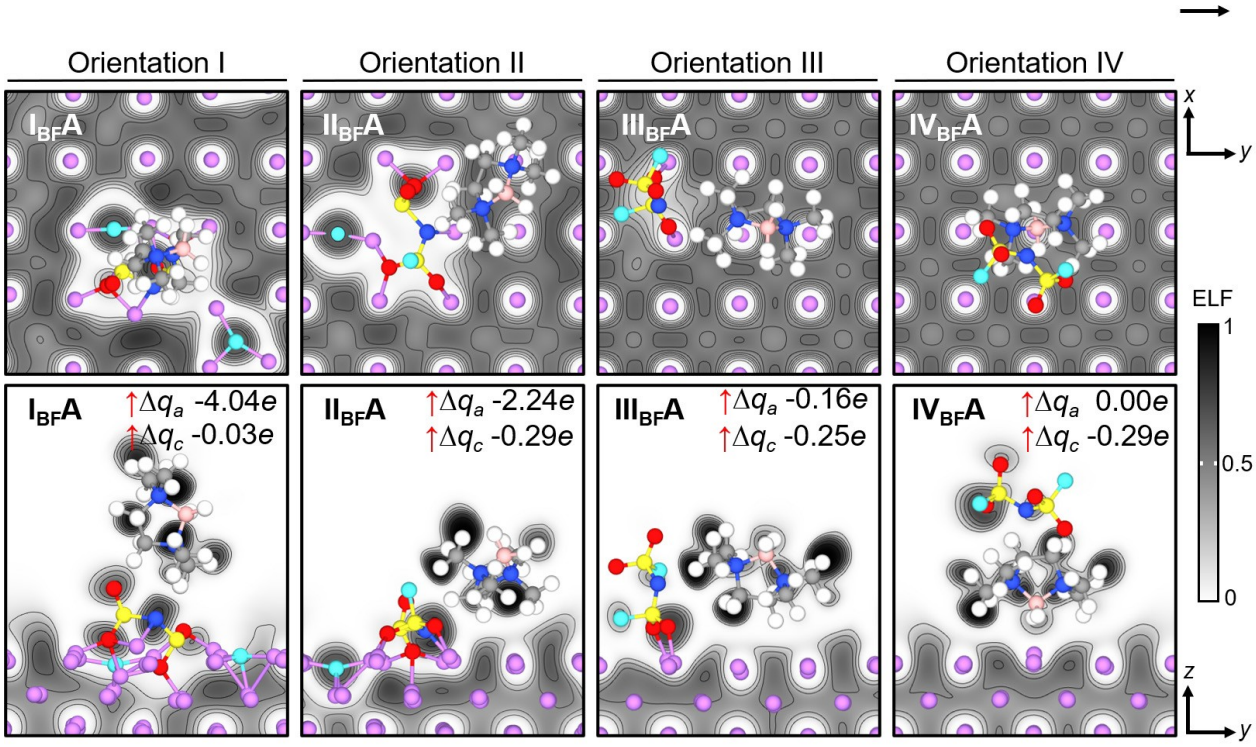

Figure 2. The most stable structures ($\mathbf{I}_{BF}\mathbf{A}$, $\mathbf{II}_{BF}\mathbf{A}$, $\mathbf{III}_{BF}\mathbf{A}$ and $\mathbf{IV}_{BF}\mathbf{A}$) for the four different orientations for the [(TMEDA)BH_2][FSI]/Li(001) systems are shown with an ELF slice cut through the top-most Li surface. High regions of ELF (values near 1) can be interpreted as bonding and nonbonding electron pairs. Δq_a and Δq_c represent the charge transferred to the anion and cation, respectively.

bonded to the Li surface via the nitrogen atom and three oxygen atoms. The cation remained intact during these steps.

For the second reaction pathway (that resulted in structure $\mathbf{I_{BF}B}$), the first step was the same as for structure $\mathbf{I_{BF}A}$, where one of the S–F bonds broke. The second step, in contrast, involved breaking of the N–S bond, resulting in the removal of the SO_2 fragment from the parent molecule. These steps are represented as follows [Eq. (3)]:

$$[(TMEDA)BH_2]^+ + [FSI]^- \rightarrow (TMEDA)BH_{2(ads)} + SO_2NSO_2F_{(ads)}$$
$$+F_{(ads)} \rightarrow (TMEDA)BH_{2(ads)} + NSO_2F_{(ads)} + SO_{2(ads)} + F_{(ads)} \quad (3)$$

The fluorine atom bonded to four surface Li atoms, the SO_2 fragment bonded to the surface via the two oxygen atoms, while the NSO_2F fragment bonded to two Li atoms via the oxygen and nitrogen atoms. Figure 3 provides a visual summary for the two different reaction shown for the $[FSI]^-$ anion. Again, the cation did not decompose during these steps.

For both structures $\mathbf{I_{BF}A}$ and $\mathbf{I_{BF}B}$, there is a pronounced difference in how the cation interacts with the surface. For the former, the ring structure is oriented perpendicular to the surface and located above the adsorbed fragments of the anion. In contrast, for structure $\mathbf{I_{BF}B}$ the cation ring structure is oriented parallel to the surface and located closer to the Li surface. This difference in orientation explains the reduced charge withdrawn by the cation in $\mathbf{I_{BF}A}$ ($-0.03e$) compared to $\mathbf{I_{BF}B}$ ($-0.31e$).

For Orientation $\mathbf{II_{BF}}$ (structures $\mathbf{II_{BF}A}$-$\mathbf{C}$), the anion again decomposed, however, dissociation of only a single fluorine atom from one of the $-SO_2$ groups occurred (as described by the first reaction step in equations (2) and (3)). The cation and anion for all three structures ($\mathbf{II_{BF}A}$-$\mathbf{C}$) adsorbed to the surface in a similar orientation, and hence, a similar amount of charge was withdrawn by the ion-pairs (2.53–2.29e).

For Orientation $\mathbf{III_{BF}}$ (structures $\mathbf{III_{BF}A}$-$\mathbf{C}$), the $[FSI]^-$ anion did not decompose and adsorbed to the Li surface via the sulfonyl oxygen atoms (or nitrogen atom in structure $\mathbf{III_{BF}C}$). The main difference between these three structures is found for structure $\mathbf{III_{BF}C}$, where the $[FSI]^-$ anion shields the cation from interacting with the Li surface. This results in the cation donating charge to the anion ($+0.03e$) as opposed to withdrawing charge from the surface, as was determined for structures $\mathbf{III_{BF}A}$-$\mathbf{B}$.

For Orientation $\mathbf{IV_{BF}}$ (structures $\mathbf{IV_{BF}A}$-$\mathbf{C}$), where the binding is the weakest (-0.24 to -0.17 eV), the cation adsorbs closest to the surface with the anion located above the cation and hence not interacting with the surface. As a result, charge transfer only occurs via the cation.

Overall, the structures with larger binding energies correlate to a greater transfer of charge from the surface to the ion-pair. Specifically, this occurred when the anion decomposed on the surface (namely for Orientations $\mathbf{I_{BF}}$ and $\mathbf{II_{BF}}$).

Again, the cyclic cation paired with $[FSI]^-$ showed similar binding properties compared to the open-chain cation with $[FSI]^-$.[19] The associated DOS (Figures S5–S8) show an overlap of states between the ion-pair and the Li surface between ~1 to ~4.5 eV, with an increase in intensity of the Li surface states occurring between ~3.75 and ~4.5 eV, similar to [(TMEDA)BH_2][TFSI]/Li(001).

When decomposition of the anion was seen (structure $\mathbf{I_{BF}A}$), a new strong peak at -3 eV is identified which is attributed to the $N(SO_2)_2$ fragment (Figure S5). For structure $\mathbf{I_{BF}B}$, the NSO_2F and SO_2 fragments contribute to the new states at -3.3 eV and -2.2 eV, respectively (Figure S5). Such prominent peaks are notably absent in the structures where only a single fluorine atom dissociated (structures $\mathbf{II_{BF}A}$-$\mathbf{C}$ (Figure S6)) or where no dissociation occurred (structures $\mathbf{III_{BF}A}$-$\mathbf{C}$ (Figure S7)). Therefore, these states are characteristic of dissociation of the anion into adsorbed $N(SO_2)_2$, NSO_2F or SO_2 species. It should be noted that while the anion remains intact in structures $\mathbf{IV_{BF}A}$-$\mathbf{C}$, there are small states lying at -3 eV (Figure S8) which are indicative of the anion being shielded from the surface by the cation. The difference in these states at -3 eV can be determined by examining the atoms contributing to the states, which in both cases are different.

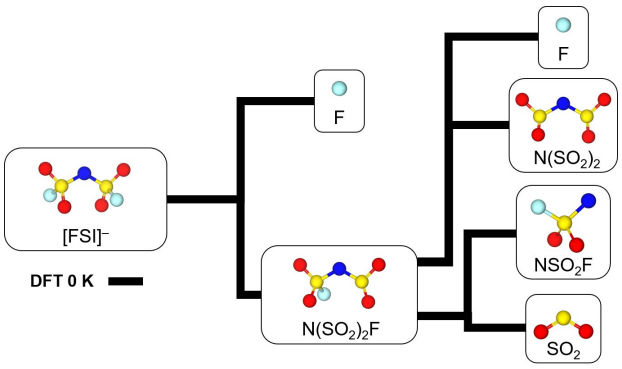

Figure 3. Decomposition pathways exhibited by the $[FSI]^-$ anion during DFT geometry optimization for [(TMEDA)BH_2][FSI]/Li(001).

2.2. AIMD Simulations of the IL/Li(001) Interface

To examine the effect of temperature on the above reactions, AIMD simulations were performed. The simulation temperatures were chosen to address (normal) LMB ambient operating temperatures (298 K) and abusive LMB usage (358 K). The most stable structures determined from **Sections 2.1.1** and **2.1.2** (namely structures $\mathbf{I_{BT}A}$ and $\mathbf{I_{BF}A}$) were used as the starting structures for the simulations.

2.2.1. [(TMEDA)BH_2][TFSI]/Li(001)

Unlike the 0 K geometry optimization calculations, $[TFSI]^-$ in structure $\mathbf{I_{BT}A}$ was shown to break down during the AIMD simulations at 298 and 358 K. Snapshots from these simulations are presented in Figure 4 and the reaction pathways in Figure 5.

At 298 K, the $-CF_3$ group of the $[TFSI]^-$ anion was shown to break away after 0.70 ps of simulation time. After a further 0.35 ps, the CF_3 broke apart into a CF_2 species and a fluorine

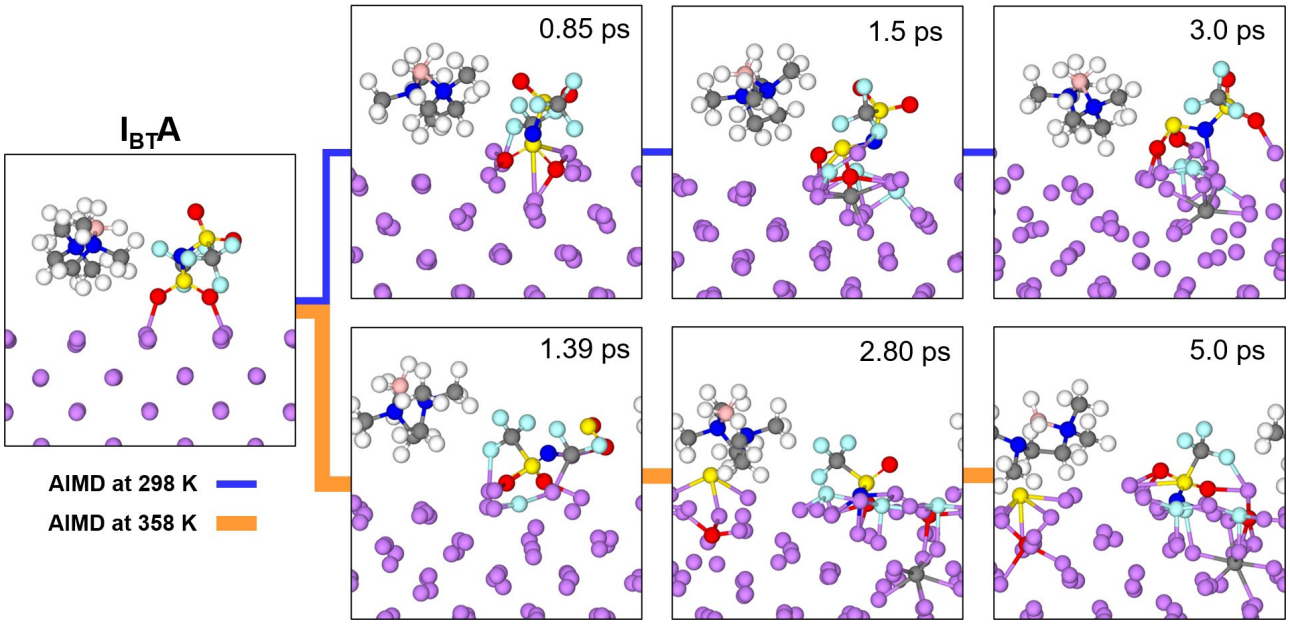

Figure 4. Snapshots from the AIMD simulations of structure $I_{BT}A$, run for 3.0 ps at 298 K (blue, thin line) and 5.0 ps at 358 K (orange, thick line).

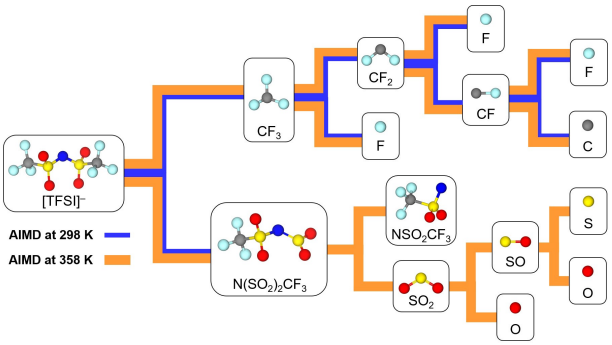

Figure 5. Decomposition pathway for $[TFSI]^-$ from the AIMD simulations at 298 K (blue, thin line) and 358 K (orange, thick line) of structure $I_{BT}A$.

atom, followed by breaking of the remaining two C–F bonds after the simulation had run for 1.35 ps and 1.45 ps.

At 358 K, the CF_3 moiety dissociates from the anion after 1.08 ps. As was also seen at 298 K, decomposition of the CF_3 followed in quick succession, forming a CF_2 and a fluorine atom after 1.2 ps. The remaining CF_2 then spontaneously breaks down into carbon and two fluorine atoms after 1.80 ps of simulation time. In contrast to the simulation at 298 K, the anion fragment $N(SO_2)_2CF_3$ dissociated further into NSO_2CF_3 and SO_2 after 1.35 ps (Figure 5). This was followed by the decomposition of the SO_2 fragment into SO and an oxygen atom after 2 ps. After 2.25 ps, the SO fragment had further decomposed into sulfur and oxygen atoms.

The decomposition of $[TFSI]^-$ during the reaction at both simulated temperatures was spontaneous, with extended fragmentation occurring at 358 K being attributed to the increased kinetics as a result of the elevated temperature. The reaction pathway seen for this system is in good agreement with what has previously been found for $[NNBH_2][TFSI]$[19] and $[Pyr_{14}][TFSI]$[15c] on Li(001), where breaking of the S–C bond is the initial reaction step. Alternatively, breaking of the S–N bond followed by S–C bond has previously been shown to occur during AIMD simulations of $[Pyr_{14}][TFSI]$/Li.[15a,c] Yet, the pathway is absent for the $[(TMEDA)BH_2][TFSI]$/Li(001) system in this work. Regardless of whether breaking of the S–C or S–N bond is the initial reaction step, eventual decomposition of the anion into atomic sulfur, oxygen, fluorine and carbon will follow.

It has previously been shown that production of key species, as a result of decomposition of the anion, is the main contributor to the composition and stability of the SEI layer on the Li electrode. The specific decomposition species include NSO_2CF_3, $-Li_2S$, $-CF_3$, LiF, SO_2, and Li_2O,[17a,30,31] which are also observedin the AIMD simulations of the boronium cation-based ILs. This may help explain the beneficial performance of such ILs.

At both temperatures, the cation remained intact during the simulation and stayed adsorbed above the surface, as was seen in the geometry optimization and for the open-chain cation.[19] A similarly weak interaction was also reported for the $[Pyr_{14}]^+$ and $[Pyr_{13}]^+$ cations with the Li(001) surface.[15b,c]

2.2.2. [(TMEDA)BH_2][FSI]/Li(001)

In contrast to the $[TFSI]^-$ based IL, the AIMD simulations of $I_{BF}A$ show no further decomposition of the $[FSI]^-$ anion fragment (or the cation) for the entire duration of the simulation at either of the reaction temperatures (Figure 6). An additional simulation at 428 K, run to simulate extreme "thermal run away" conditions also showed no decomposition of the IL (Figure S10).

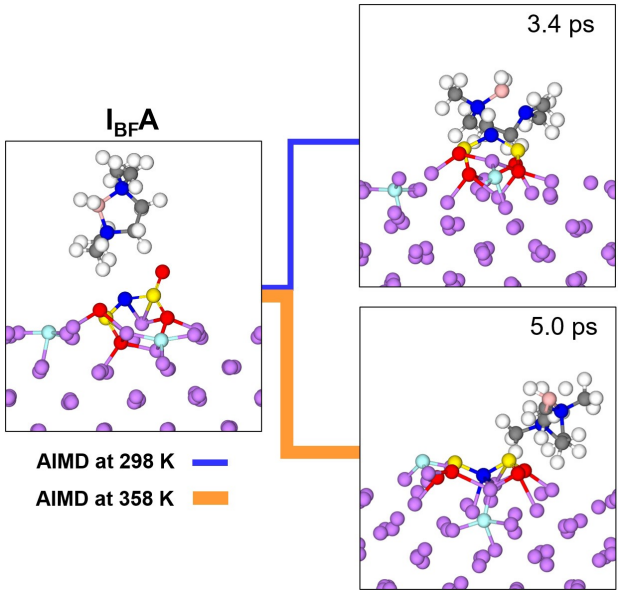

Figure 6. Snapshots of the final geometry from the AIMD simulation of structure $\mathbf{I_{BF}A}$, at 298 K (blue, thin line) for 3.4 ps and 358 K (orange, thick line) for 5.0 ps.

The reason there is no further decomposition observed may be attributed to the stability of the adsorbed $N(SO_2)_2$ fragment of the $[FSI]^-$ anion, which prevents decomposition into elemental oxygen, sulfur and nitrogen atoms. This is in contrast to the reaction path in equation (3), where previous studies[15b,19] have shown the anion fragments formed (e.g. SO_2, NSO_2 and SO_2F) to dissociate into elemental oxygen and sulfur.[15c] The prevalence of fluoride free fragments of $[FSI]^-$, such as NSO_2 or $N(SO_2)_2$ shown in this work, is supported by previous Fourier transform infrared (FTIR) spectroscopy of the SEI layer formed with $[P_{111i4}][FSI]$/Li[FSI].[10a] Previous work has shown that the formation of a predominantly mineral-based inner SEI layer assists in the formation of a stable layer.[15b,32] The fact that rapid defluorination of $[FSI]^-$ and subsequent formation of LiF species is seen in this work, supports the benefit of using boronium cation-based ILs which contain $[FSI]^-$.

The decomposition pathway of the $[FSI]^-$ anion reported in this manuscript is similar to those identified for $[NNBH_2][FSI]$[19] and $[Pyr_{13}][FSI]$.[15b] Similarly, the breakdown of the $[TFSI]^-$ anion proceeds in a similar manner to $[NNBH_2][TFSI]$[19] and $[Pyr_{14}][TFSI]$[15a,c] on the Li(001) surface at 298 K.[15,19] Additionally, the binding energy of the $[(TMEDA)BH_2][TFSI]$, $[NNBH_2][TFSI]$[19] and $[Pyr_{14}][TFSI]$[15c] cations to the Li(001) surface are similar in magnitude, hence, the presence of the IL cation in the ion-pair does not seem to modify or influence the decomposition pathway of the $[TFSI]^-$ anion at the Li(001) surface.

2.3. Possible Decomposition Reactions for the $[(TMEDA)BH_2]^+$ Cation

Even though the AIMD simulations did not show decomposition of the cation, it is possible that a longer simulation time may be needed to see such an event. We therefore used constrained geometry optimization calculations to determine the energy required for removal of a hydrogen atom from either the BH_2 center or the $-CH_3$ groups. From these calculations it is possible to focus on removing a hydrogen atom from the $-BH_2$ or $-CH_3$ group using one of the $[(TMEDA)BH_2][TFSI]$/Li(001) structures, $\mathbf{I_{BT}D}$. The magnitude of the energy barrier gives an indication of the likelihood of removing these hydrogen atoms. The optimized structure $\mathbf{I_{BT}D}$ was chosen as the initial reaction state based on the orientation of the cation, which had hydrogen atoms from both the $-BH_2$ and $-CH_3$ groups directed towards the Li surface atoms. The reaction pathways examined are shown in Figure 7, with the difference in energy between the initial and final states providing the reaction energy, ΔE.

Images 1–3 are representative of the dissociation of the hydrogen atom from the parent molecule, with the activation energy (E_A) for the breaking of the B–H or C–H represented by Image 1 (Figure 7a) and Image 2 (Figure 7b), respectively. Additionally, the possible reaction rate for breaking of the B–H and C–H bonds can be estimated using the Arrhenius equation [Eq. (4)]:

$$R_r = k_0 \dot{s} \exp(-E_A/k_b T) \quad (4)$$

where R_r is the reaction rate per second, k_0 is the exponential prefactor (using 10^{12}, a typical molecular vibrational frequency), E_A is the activation energy, k_b is the Boltzmann constant and T is the temperature (298 K). To estimate the reaction rate, we assume an Arrhenius behaviour of the reactions and ignore entropic effects. A comparison of the activation energies and reaction rates for the cyclic and open-chain[19] boronium cations are shown in Table 1.

Cleavage of both the B–H and C–H bonds in $[(TMEDA)BH_2]^+$ show an activation energy of +0.61 and +0.76 eV, respectively. These values are lower compared to the equivalent reactions in the $[NNBH_2]^+$ cation, previously determined to be +0.97 eV (B–H) and +1.02 eV (C–H).[19] These lower activation energies for the cyclic cation translate into an increased reaction rate of ~48 and ~0.14 reactions/s (Table 1), for the breaking of a single B–H and C–H bond, respectively (equivalent to ~0.02 and

Table 1. Activation energies (E_A) and estimated reaction rates (R_r) for breaking of the B–H and C–H bonds on the boronium cations $[(TMEDA)BH_2]^+$ and $[NNBH_2]^+$ at 298 K. Activation energies for $[NNBH_2]^+$ are provided by Ref. [19].

[cation][anion]/Li(001)	B–H Breaking		C–H Breaking	
	E_A [eV]	R_r [reactions/s]	E_A [eV]	R_r [reactions/s]
$[(TMEDA)BH_2][TFSI]$/Li(001)	+0.61	~48	+0.76	~0.14
$[NNBH_2][TFSI]$/Li(001)[19]	+0.97	$\sim 4\times10^{-5}$	+1.02	$\sim 6\times10^{-6}$

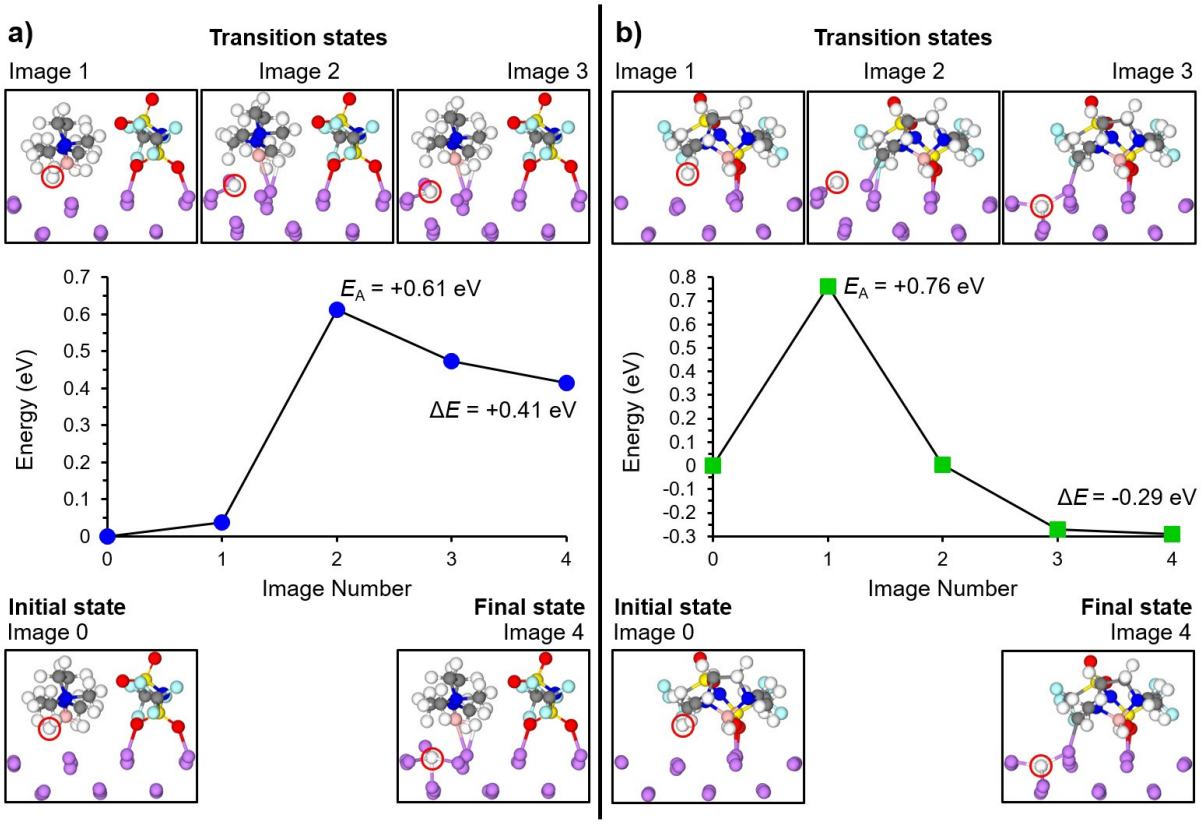

Figure 7. Reaction profiles for a) B–H or b) C–H bond breaking from the $-BH_2$ or $-CH_3$ groups of $[(TMEDA)BH_2]^+$ on the Li(001) surface using structure $\mathbf{I_{BT}D}$.

~7 seconds for a single reaction to occur). For the $[NNBH_2]^+$ cation, the reaction rate is significantly slower (~4×10^{-5} and ~6×10^{-6} reactions/s), which is equivalent to ~7 (B–H) and ~49 hours (C–H) for a single reaction on the Li surface.

As the activation energies are lower (resulting in higher estimated reaction rates) for the decomposition of $[(TMEDA)BH_2]^+$ than for $[NNBH_2]^+$, this suggests that hydrogen abstraction could occur more readily for the cyclic cation compared to the open-chain derivative.

The relative stability demonstrated by the cyclic and open chain[19] boronium cations with the Li(001) surface could be a critical feature for extending the cycle life of Li metal-based batteries. Characterization of the SEI layer composition for $[Pyr_{14}][TFSI]$ and $[Pyr_{13}][FSI]$ IL-based electrolytes has previously identified decomposition products attributed to the quaternary pyrrolidinium cations due to Hofmann β-elimination reactions.[2a,18] In contrast, this elimination process does not apply to the tertiary amines coordinating in the boronium cations, hence, they are more likely to remain intact, possibly embedded in the SEI layer, similar to the phosphonium $[P_{111i4}]^+$ cation.[10a]

These differences in the chemical stability of the boronium and pyrrolidinium cations, as well as the different composition of their respective SEI layers, may explain the improved cycling stability and capacities previously demonstrated for $[NNBH_2][TFSI]+0.5\ mol\cdot kg^{-1}$ Li[TFSI] as opposed to the equivalent $[Pyr_{14}][TFSI]$ electrolyte.[3a]

3. Conclusions

The reactions between the ionic liquids, $[(TMEDA)BH_2][TFSI]$ and –[FSI] and the Li metal anode, that lead to SEI layer formation, have been examined using DFT calculations and AIMD simulations. Both the two anions and the cation were found to accept charge from the surface upon adsorption, indicating that they are susceptible to reduction by the Li electrode. Following adsorption on the Li surface, decomposition of both anions occurs spontaneously, forming the initial components of the SEI layer, which have been identified to include LiF and Li_xO species. In contrast to the anions, decomposition of the cation is not facile and instead was shown to only interact weakly with the electrode surface. This suggests the cation is unlikely to participate in the formation of the inner inorganic layer of a passivation film on the Li metal anode. The relatively low activation energy for hydrogen abstraction from the $-BH_2$ and $-CH_3$ groups of the cation, however, compared to the open-chain derivative ($[NNBH_2]^+$), indicates the former may have a greater influence on the SEI layer composition than the latter. Surface characterization of the SEI layer formed on the Li surface using these ionic liquids is currently underway to validate the predicted stability of the $[(TMEDA)BH_2]^+$ cation on the Li metal anode. Overall, the similar electronic properties and adsorption behavior of $[(TMEDA)BH_2]^+$ studied here, when compared to the established $[NNBH_2]^+$ cation indicates the former can be considered another viable boronium IL cation for use in LMB electrolytes.

Acknowledgements

This work was supported by computational resources provided by the Australian Government through NCI, Pawsey and MASSIVE, under the National Computational Merit Allocation Scheme and through the Pawsey Energy and Resources Merit Allocation Scheme. This work was funded in part by the CSIRO AIM Future Science Platform. P.J. would like to acknowledge several of Chalmers Areas of Advance: Materials Science, Energy, and Transport, for continuous support, and the Swedish Energy Agency for grant #P39909-1.

Conflict of Interest

The authors declare no conflict of interest.

Keywords: Li metal anode · ionic liquids · boronium cation · SEI layer · lithium battery

[1] a) M. D. Tikekar, S. Choudhury, Z. Tu, L. A. Archer, *Nat. Energy* **2016**, *1*, 16114; b) M. D. Brennan, M. Breedon, A. S. Best, T. Morishita, M. J. S. Spencer, *Electrochim. Acta* **2017**, *243*, 320–330.

[2] a) A. Basile, A. I. Bhatt, A. P. O'Mullane, *Nat. Commun.* **2016**, *7*, 11794; b) B. Tong, X. Chen, L. Chen, Z. Zhou, Z. Peng, *ACS Appl. Mater. Interfaces* **2018**, *1*, 4426–4431; c) N. W. Li, Y. X. Yin, J. Y. Li, C. H. Zhang, Y. G. Guo, *Adv. Sci.* **2017**, *4*, 1600400; d) P. Jankowski, W. Wieczorek, P. Johansson, *Energy Storage Mater.* **2019**, *20*, 108–117.

[3] a) T. Rüther, T. D. Huynh, J. Huang, A. F. Hollenkamp, E. A. Salter, A. Wierzbicki, K. Mattson, A. Lewis, J. H. Davis, *Chem. Mater.* **2010**, *22*, 1038–1045; b) Y. Yang, F. Men, Z. Song, Y. Zhou, H. Zhan, *Electrochim. Acta* **2017**, *256*, 37–43; c) A. I. Bhatt, A. S. Best, J. Huang, A. F. Hollenkamp, *J. Electrochem. Soc.* **2010**, *157*, A66-A74.

[4] D.-J. Yoo, K. J. Kim, J. W. Choi, *Adv. Energy Mater.* **2018**, *8*, 1702744.

[5] M. C. Kroon, W. Buijs, C. J. Peters, G.-J. Witkamp, *Green Chem.* **2006**, *8*, 241–245.

[6] M. Pyschik, C. Schultz, S. Passerini, M. Winter, S. Nowak, *Electrochim. Acta* **2015**, *176*, 1143–1152.

[7] a) Z. Zhang, P. Zhang, Z. Liu, B. Du, Z. Peng, *ACS Appl. Mater. Interfaces* **2020**, *12*, 11635–11642; b) Z. Liu, J. Huang, Y. Zhang, B. Tong, F. Guo, J. Wang, Y. Shi, R. Wen, Z. Zhou, L. Guo, Z. Peng, *Adv. Energy Mater.* **2019**, *9*, 1901967; c) U. Ulissi, G. A. Elia, S. Jeong, F. Mueller, J. Reiter, N. Tsiouvaras, Y. K. Sun, B. Scrosati, S. Passerini, J. Hassoun, *ChemSusChem* **2018**, *11*, 229–236; d) C. A. Calderón, A. Vizintin, J. Bobnar, D. E. Barraco, E. P. M. Leiva, A. Visintin, S. Fantini, F. Fischer, R. Dominko, *ACS Appl. Mater. Interfaces* **2020**, *3*, 2020–2027.

[8] a) J. S. Moreno, Y. Deguchi, S. Panero, B. Scrosati, H. Ohno, E. Simonetti, G. B. Appetecchi, *Electrochim. Acta* **2016**, *191*, 624–630; b) G. A. Elia, J. Hassoun, W. J. Kwak, Y. K. Sun, B. Scrosati, F. Mueller, D. Bresser, S. Passerini, P. Oberhumer, N. Tsiouvaras, J. Reiter, *Nano Lett.* **2014**, *14*, 6572–6577; c) G. A. Elia, U. Ulissi, S. Jeong, S. Passerini, J. Hassoun, *Energy Environ. Sci.* **2016**, *9*, 3210–3220; d) J. R. Nair, F. Colò, A. Kazzazi, M. Moreno, D. Bresser, R. Lin, F. Bella, G. Meligrana, S. Fantini, E. Simonetti, G. B. Appetecchi, S. Passerini, C. Gerbaldi, *J. Power Sources* **2019**, *412*, 398–407; e) H. Lu, Y. Zhu, B. Zheng, H. Du, X. Zheng, C. Liu, Y. Yuan, J. Fang, K. Zhang, *New J. Chem.* **2020**, *44*, 361–368.

[9] a) J. Zhang, B. Sun, Y. Zhao, A. Tkacheva, Z. Liu, K. Yan, X. Guo, A. M. McDonagh, D. Shanmukaraj, C. Wang, T. Rojo, M. Armand, Z. Peng, G. Wang, *Nat. Commun.* **2019**, *10*, 602; b) A. Tsurumaki, H. Ohno, S. Panero, M. A. Navarra, *Electrochim. Acta* **2019**, *293*, 160–165; c) F. Liang, J. Yu, D. Wang, L. Dong, C. Ma, J. Chen, B. Yang, C. Zhu, Y. Gao, C. Li, *Electrochim. Acta* **2019**, *307*, 83–91; d) X. Pan, T. Liu, D. J. Kautz, L. Mu, C. Tian, T. E. Long, P. Yang, F. Lin, *J. Power Sources* **2018**, *403*, 127–136; e) M. A. Navarra, K. Fujimura, M. Sgambetterra, A. Tsurumaki, S. Panero, N. Nakamura, H. Ohno, B. Scrosati, *ChemSusChem* **2017**, *10*, 2496–2504.

[10] a) G. M. A. Girard, M. Hilder, N. Dupre, D. Guyomard, D. Nucciarone, K. Whitbread, S. Zavorine, M. Moser, M. Forsyth, D. R. MacFarlane, P. C. Howlett, *ACS Appl. Mater. Interfaces* **2018**, *10*, 6719–6729; b) X. Lin, R. Kavian, Y. Lu, Q. Hu, Y. Shao-Horn, M. W. Grinstaff, *Chem. Sci.* **2015**, *6*, 6601–6606.

[11] J. H. Davis, Jr., T. Rüther, S. Dorman, in *PRiME 2012, Vol. 50* (Eds.: W. M. Reichert, D. M. Fox, R. A. Mantz, M. Mizuhata, P. C. Trulove, H. De Long, A. Ispas, A. Bund), ECS Transactions, Honolulu, Hawaii, **2012**, pp. 293–299.

[12] G. M. A. Girard, M. Hilder, D. Nucciarone, K. Whitbread, S. Zavorine, M. Moser, M. Forsyth, D. R. MacFarlane, P. C. Howlett, *J. Phys. Chem. C* **2017**, *121*, 21087–21095.

[13] a) L. Liu, J. Park, X. Lin, A. M. Sastry, W. Lu, *J. Power Sources* **2014**, *268*, 482–490; b) M. Broussely, S. Herreyre, P. Biensan, P. Kasztejna, K. Nechev, R. J. Staniewicz, *J. Power Sources* **2001**, *97–98*, 13–21; c) A. Wang, S. Kadam, H. Li, S. Shi, Y. Qi, *NPJ Comp. Mat.* **2018**, *4*; d) N. Takenaka, Y. Suzuki, H. Sakai, M. Nagaoka, *J. Phys. Chem. C* **2014**, *118*, 10874–10882.

[14] D. Aurbach, I. Weissman, A. Schechter, H. Cohen, *Langmuir* **1996**, *12*, 3991–4007.

[15] a) B. V. Merinov, S. V. Zybin, S. Naserifar, S. Morozov, J. Oppenheim, W. A. Goddard, J. Lee, J. H. Lee, H. E. Han, Y. C. Choi, S. H. Kim, *J. Phys. Chem. Lett.* **2019**, *10*, 4577–4586; b) A. Budi, A. Basile, G. Opletal, A. F. Hollenkamp, A. S. Best, R. J. Rees, A. I. Bhatt, A. P. O'Mullane, S. P. Russo, *J. Phys. Chem. C* **2012**, *116*, 19789–19797; c) H. Yildirim, J. B. Haskins, C. W. Bauschlicher, J. W. Lawson, *J. Phys. Chem. C* **2017**, *121*, 28214–28234.

[16] a) G. H. Lane, P. M. Bayley, B. R. Clare, A. S. Best, D. R. MacFarlane, M. Forsyth, A. F. Hollenkamp, *J. Phys. Chem. C* **2010**, *114*, 21775–21785; b) D. Aurbach, I. Weissman, A. Zaban, O. Chusid, *Electrochim. Acta* **1994**, *39*, 51–71; c) P. C. Howlett, N. Brack, A. F. Hollenkamp, M. Forsyth, D. R. MacFarlane, *J. Electrochem. Soc.* **2006**, *153*, A595.

[17] a) P. C. Howlett, D. R. MacFarlane, A. F. Hollenkamp, *Electrochem. Solid-State Lett.* **2004**, *7*, 97–101; b) J. Zheng, M. Gu, H. Chen, P. Meduri, M. H. Engelhard, J.-G. Zhang, J. Liu, J. Xiao, *J. Mater. Chem. A* **2013**, *1*, 8464–8470.

[18] Y. Preibisch, F. Horsthemke, M. Winter, S. Nowak, A. S. Best, *Chem. Mater.* **2020**, *32*, 2389–2398.

[19] J. Clarke-Hannaford, M. Breedon, T. Rüther, M. J. S. Spencer, *ACS Appl. Mater. Interfaces* **2020**, *3*, 5497–5509.

[20] F. Begum, M. A. Choudhary, M. A. Mirza, B. Twamley, R. J. Baker, *J. Chem. Crystallogr.* **2018**, *48*, 209–212.

[21] a) G. Kresse, J. Furthmuller, *Phys. Rev. B* **1996**, *54*, 11169–11186; b) G. Kresse, J. Furthmuller, *Comput. Mater. Sci.* **1996**, *6*, 15–50; c) G. Kresse, J. Hafner, *Phys. Rev. B* **1993**, *47*, 558–561; d) G. Kresse, D. Joubert, *Phys. Rev. B* **1999**, *59*, 1758–1775.

[22] P. E. Blöchl, *Phys. Rev. B: Condens. Matter Mater. Phys.* **1994**, *50*, 17953–17979.

[23] J. P. Perdew, K. Burke, M. Ernzerhof, *Phys. Rev. Lett.* **1996**, *77*, 3865–3868.

[24] S. Grimme, J. Antony, S. Ehrlich, H. Krieg, *J. Chem. Phys.* **2010**, *132*, 154104.

[25] J. Clarke-Hannaford, M. Breedon, A. S. Best, M. J. S. Spencer, *Phys. Chem. Chem. Phys.* **2019**, *21*, 10028–10037.

[26] a) W. Tang, E. Sanville, G. Henkelman, *J. Phys. Condens. Matter* **2009**, *21*, 084204; b) G. Henkelman, A. Arnaldsson, H. Jónsson, *Comput. Mater. Sci.* **2006**, *36*, 354–360.

[27] A. D. Becke, K. E. Edgecombe, *J. Chem. Phys.* **1990**, *92*, 5397–5403.

[28] S. Nosé, *J. Chem. Phys.* **1984**, *81*, 511–519.

[29] S. Kabekkodu, *International Center for Diffraction Data*, ICCD 2018, PDF-4+, Newton Square, PA, USA, **2018**.

[30] S. Xiong, K. Xie, E. Blomberg, P. Jacobsson, A. Matic, *J. Power Sources* **2014**, *252*, 150–155.

[31] J. Zheng, M. Gu, H. Chen, P. Meduri, M. H. Engelhard, J.-G. Zhang, J. Liu, J. Xiao, *J. Mater. Chem. A* **2013**, *1*, 8464–8470.

[32] I. A. Shkrob, T. W. Marin, Y. Zhu, D. P. Abraham, *J. Phys. Chem. C* **2014**, *118*, 19661–19671.

Manuscript received: January 28, 2021
Revised manuscript received: March 29, 2021
Accepted manuscript online: March 30, 2021
Version of record online: April 15, 2021